Structural Flexibility and Electronic Tuning in N5-Substituted Anionic Reduced Flavins: Implications for Flavoenzyme Intermediates

Nadia Dozova, Fabien Lacombat, Pascal Plaza, Djemel Hamdane, Bruno Madebène

Structural Flexibility and Electronic Tuning in N_5-Substituted Anionic Reduced Flavins: Implications for Flavoenzyme Intermediates

Nadia Dozova,*[a] Fabien Lacombat,[a] Pascal Plaza,[a] Djemel Hamdane*[b] and Bruno Madebène*[c]

[a] *PASTEUR, Département de chimie, École normale supérieure, PSL University, Sorbonne Université, CNRS, 75005 Paris, France.*

[b] *Laboratoire de Chimie des Processus Biologiques, CNRS-UMR 8229, Collège de France, Sorbonne Université, 75005 Paris, France.*

[c] *Sorbonne Université CNRS, MONARIS, UMR8233, F-75005 Paris, France*

† Electronic supplementary information (ESI) available. See DOI:

ABSTRACT

N_5-substituted reduced flavins are pivotal and yet underexplored intermediates in flavoenzyme catalysis, which hold untapped potential for advancing enzymatic and catalytic processes. Here, we combine steady-state and ultrafast transient absorption spectroscopy with DFT/TDDFT simulations to explore the structural and electronic dynamics of several non-fluorescent anionic reduced flavin derivatives involved in flavoenzyme processes. Unlike the broad, featureless absorption spectrum of $FADH^-$, N_5-substituted flavins exhibit distinct blue-shifted absorption bands at 330 nm or 370 nm, reflecting substantial electronic reorganization. Our theoretical results challenge the conventional view that isoalloxazine ring bending along the N_5-N_{10} axis governs the absorption properties of the molecule, and demonstrate instead that HOMO orbital stabilization is the critical factor. Ultrafast spectroscopy reveals transient absorption bands above 450 nm, corresponding to different isoalloxazine bend conformations, which converge into a single band at ~500 nm within tens of picoseconds. This evolution is assigned to a rapid structural relaxation toward a more planar configuration. Along this path the system relaxes to the ground state through a conical intersection (CI) whose position is modulated by the nature of the N_5 substituent. These findings fundamentally reshape our understanding of flavin photophysics.

1. INTRODUCTION

Flavin adenine dinucleotide (FAD, compound **1** in Fig. 1) is the biological cofactor of a large number of flavoproteins. It is involved in a plethora of chemical reactions such as electron, proton, hydride, oxo or methylene transfer,[1-5] which makes it one of the most versatile bioorganic catalysts. The origin of this versatility lies in the unique ability of the isoalloxazine moiety to (i) exist under three readily accessible redox forms (oxidized, semi-reduced and fully reduced) and associated protonation states and to (ii) undergo electronic excitation upon irradiation by visible light.[6-9] This photophysical feature gives rise to original photoinduced reactivities such as those observed in several blue-light photoreceptors,[10] DNA repair catalyzed by photolyases,[11] or photodecarboxylation of free fatty acids.[12]

Unlike other redox forms, the fully reduced flavin has a distinctive non-planar isoalloxazine.[13-24] This structural feature seems to have an important functional role depending on the enzyme systems.[25] The isoalloxazine bending occurs along the N_5-N_{10} short axis, with a bend angle lying between *ca.* 8° and 28° (depending on the source and protonation state) and strongly affected by the environment of the molecule.[13-24] Some lower values (*ca.* 2-18°) have been reported inside reduced flavoproteins,[26-28] which suggests that flavoproteins have the ability to modulate the isoalloxazine bending for functional purposes. The energy barrier for ring inversion along the bending coordinate, commonly referred to as butterfly motion, has indeed been estimated to be relatively low (2-4.8 kcal/mol) in different reduced flavins.[14-16,18] In addition to X-ray crystallography, methods like NMR spectroscopy and theoretical calculations provide valuable insights into the ground-state conformation of flavins. Meanwhile, ultrafast spectroscopy offers detailed information about the butterfly motion dynamics in the excited state, revealing how environmental constraints, particularly in flavoproteins, influence isoalloxazine behavior. For example, while the excited state of $FADH^-$ in solution is very short-lived (multiexponential decay with average decay time constant in the range of 8-25 ps),[8,29-34] it becomes much slower (0.6-3 ns) when the flavin is imbedded in a rigid protein environment.[35-41] The butterfly coordinate has been invoked to explain the rapid excited-state decay of $FADH^-$ in solution. Continuous motion along this coordinate in the excited state has been proposed to lead to a conical intersection (CI) with the ground state, where deactivation occurs.[39] In the environment of rigid flavoproteins (*e.g.* photolyase, cryptochrome) this motion is strongly hindered, thereby explaining the much enhanced excited-state lifetime.[39] Intermediate lifetimes (tens to hundreds of ps) were recently reported by Dozova *et al.*[34] using thymidylate synthase ThyX,[42,43] in the presence or absence of its folate and dUMP substrates, to modulate steric hindrance in the flavin environment. The observed behavior is in qualitative agreement with the butterfly-motion mechanism. However, when $FADH^-$ is sandwiched between the folate and dUMP substrates,

the excited-state decay of $FADH^-$ is surprisingly faster than with only one of the substrates. It was suggested that the environment might not only affect the dynamics along the excited state surface but also alter the geometry of the CI itself and, consequently, the amount of deformation needed to reach it. Little is yet known about the actual configuration of the CI, possibly highly distorted according to a couple theoretical calculations.[44,45] When suitably stabilized in a constrained environment, excited $FADH^-$ may on the other hand act as a reductant, as in the DNA repair mechanism of photolyases, where photoinduced electron transfer to the DNA lesion initiates the repair process.[46,47]

N_5-substituted reduced flavins form a group of much less studied compounds even though they are known to be involved in the catalytic cycle of a number of flavoenzymes,[48-58] or produced by flavoenzyme inhibitors.[59] The time-resolved photophysical behavior of these compounds has not yet been investigated, to the best of our knowledge. In the present work, we aim at filling this gap and focus on two N_5-substituted derivatives of $FADH^-$ acting as a methylene donor in two methyltransferases, namely the aforementioned ThyX[42,43] and TrmFO,[54,60] a bacterial flavin-dependent tRNA methyltransferase. Crystallographic evidence suggests that the "butterfly movement" of flavin is a critical mechanism, enabling the controlled, unidirectional transfer of activated methylene groups between the initial carbon donor (folate) and the acceptor substrate (dUMP or tRNA).[34] Moreover, during the carbon transfer reaction of ThyX, a transient flavin carbinolamine intermediate (compound **2** in Fig. 1) plays an essential enzymatic role, facilitating the transfer from folate to dUMP.[61] In contrast, TrmFO has been shown to form a covalently-bound thioester intermediate, in which reduced FAD is linked to an active site cysteine residue. A simplified mimic of this adduct, where the cysteine is replaced with a thiomethyl group, is represented by compound **3** in Fig. 1 (with the actual TrmFO adduct denoted as **3O**). Here, we present an exhaustive spectroscopic, dynamical and theoretical characterization of these enzyme intermediates (**2** and **3**). To further explore the reduced FAD environment, we synthesized and analyzed two additional derivatives, compounds **4** and **5**, which feature modifications of the N_5 substituent of compound **3**, with nitrile and phenyl moieties replacing the terminal methyl group, respectively (see Fig. 1). The electronic structures, photophysics and dynamics of these compounds were investigated by steady-state UV-vis absorption and femtosecond transient absorption spectroscopy in aqueous solution. Additionally, we employed DFT and TDDFT calculations to model their ground- and excited-state structures, optical transitions, and UV-vis absorption spectra, using lumiflavin analogs (R = CH_3 in Fig. 1, denoted as **1'**, **2'**, and **3'**) embedded in an explicit aqueous environment.

2. MATERIALS AND METHODS

2.1. Samples preparation

Since the adducts **2**-**5** are quickly oxidized in the presence of O_2 (like reduced FAD **1**), all experiments were performed under anaerobic conditions.

Of note, compounds **2** and **3** were previously synthesized using a previously published protocol.[60,61] Their structures were confirmed by mass spectrometry, UV/Visible spectroscopy, and X-ray crystallography.[60,61] The other related compounds were obtained using a similar protocol. Briefly, Compound **1** ($FADH^-$) was used as a starting building block of all N_5 adducts. It was prepared by reducing FAD_{ox} (Sigma-Aldrich) in phosphate buffer (0.1 M) at pH 8, adding stoichiometric quantities of sodium dithionite.[6,31,60] Steady-state absorption spectroscopy (Cary 300, Varian) was used to monitor the titration and stop the reaction at the equivalence point.

Compound **2** was synthesized by adding a large excess (20 equivalents) of formaldehyde to **1.** The different variants of **3-5** were synthesized as follows: FAD_{ox} was reduced by a large excess of sodium dithionite (20 equivalents) in the presence of large excess of the corresponding $Cl\text{-}CH_2\text{-}S\text{-}R$ reactant (200 equivalents) (Sigma-Aldrich: chloromethyl methyl sulfide for **3**, chloromethyl thiocyanate for **4** and chloromethyl phenyl sulfide for **5**) for one hour. The solution was washed three times with dichloromethane in order to extract any excess reactants from the aqueous solution including excess sodium dithionite. Compound **5** was not fully soluble in water nor in any usual alcohols. A mixture of 50% buffer and 50% acetonitrile was used instead, which might induce different solvatochromic effects from the sole phosphate buffer for the other compounds. Steady-state spectroscopy was used to confirm the formation and stability of the products.

All samples were kept at 10 °C with the help of a circulating thermostat bath.

2.2. Femtosecond transient absorption spectroscopy

Transient absorption spectra were recorded by the pump-probe technique, with a white-light continuum probe, as previously described.[34] In brief, the pump pulses (50 fs) were tuned at 360 nm by sum frequency generation. The excitation energy (~70 nJ, focused on a surface of ~12000 μm^2) was chosen to lie in the linear regime. The excited fraction of the samples was calculated[62] to be in the order of 1-2%. The (linear) polarizations of the pump and probe beams were set at the magic angle. All transient spectra are presented as difference spectra, between pumped and unpumped absorbances (ΔA), between 330 and 790 nm.

The transient absorption data were globally fitted to a discrete sum of exponential functions, in some cases followed by a plateau, convoluted by a Gaussian function representing the instrument response function (~100 fs, full width at half maximum). The global fits yield time constants (Table 1)

and decay-associated difference spectra (DADS; ESI,† Section S2.2). The latter were used to build so-called evolution-associated difference spectra (EADS, ESI,† Section S2.3),[63] which correspond to a formal cascading model with unit quantum yield between successive states (not to be considered as an actual kinetic model of the reactivity). Note that EADS1 represents the initial transient spectrum, extrapolated at t=0 after deconvolution of the instrument response function; it may thus show some differences with the raw spectra at early times.

The overall excited-state decay was further determined by integrating the transient spectra between 380 and 700 nm to smooth out the spectral changes occurring while the transient population evolves on the excited-state surface. The obtained kinetic traces (given in ESI,† Section S2.5) were then fitted to a sum of exponentials (Table 2). The average decay time ($\overline{\tau}$) and standard deviation of decay times (σ) were finally calculated (Table 3) using the fitted parameters. The full procedure is detailed in Ref. [34].

Let us note that we actually believe the transient absorption evolutions we observed are continuous ones, in line with the interpretation background outlined in the Introduction (butterfly motion towards a CI). It is therefore most likely that this continuous evolution is somewhat artificially captured as a multiexponential behavior by the above data analysis methods. This is the reason why a precise meaning of each time component will not be sought.

2.3. Theoretical calculations

Density functional theory (DFT) and time dependent density functional theory (TDDFT) calculations were performed using the Gaussian 16 quantum chemical packages.[64] Geometries optimizations were carried out using PBE1PBE and CAM-B3LYP functionals.[65] D3 version of Grimme's dispersion with Becke-Johnson damping (GD3BJ) has been used with both functionals.[66] The Pople triple-zeta quality basis set extended with polarization and diffuse functions 6-311++G(d,p) has been used for all DFT and TDDFT calculations.[67]

Implicit and explicit solvent models were used. Polarizable Continuum Model (PCM) was used for implicit water solvation, as parameterized in Gaussian 16. As lumiflavin analogs present too many proton acceptor and donor sites to consider a simple explicit treatment of the solvation by judicious positioning of a few water molecules, the following procedure was used for explicit solvation treatment:

a) The quantum cluster grow (QCG)[68] method from the Conformer-Rotamer Ensemble Sampling Tool code (CREST)[69,70] was used with GFN2-xTB[71] semi-empirical extended tight binding method (xTB) to coat lumiflavin analogs **1'**, **2'** and **3'** with 150 to 200 water molecules to ensure 2 solvation layers;

b) Conformational ensemble generation and the search for the minimum conformations of the microhydrated clusters were then performed with the non-covalent mode (NCI) of CREST and GFN2-xTB;
c) From the most stable structures, water molecules were then removed to keep only the first water shell around lumiflavin derivatives (29, 40 and 44 waters molecules for respectively **1'**, **2'** and **3'**);
d) Final structures were then optimized with both PBE1PBE and CAM-B3LYP functionals, and TDDFT calculations were performed with the same computational methods.

All UV-Visible spectra were plotted from TDDFT calculations using GaussView and standard parameters (a gaussian with half-width at half height of 0.333 eV (2686 cm^{-1})) without any scaling or shift correction on wavelength.[72]

Atomic charges have been calculated according to two paradigms: Bader's charge and Natural population analysis (NPA). Bader's charge calculations have been performed with Topchem2 from .wfx files generated with Gaussian 16.[73,74] Natural population analysis (NPA) has been performed with NBO6.[75]

3. RESULTS

For the sake of clarity, we hereunder present bare experimental results without interpretation, followed by the results of our theoretical calculations. Interpretations and links between the two approaches are made in the Discussion Section.

3.1. Steady-state optical spectroscopy

As a preamble, let us recall that the absorption of reduced flavins in the near UV and visible range has been shown to be composed of three close-lying transitions,[6,23,35,76] noted here T_1 to T_3 from red to blue[†]. These transitions are for instance well distinguished at 415 nm (T_1), 356 nm (T_2) and 296 nm (T_3) for anionic reduced tetraacetyl riboflavin in ethanol at 77 K.[6] At room temperature or in $FADH^-$ (**1**) in aqueous solution, these bands are highly broadened and reduced to shallow structures (see Fig. 2).

Fig. 2 shows steady-state absorption spectra of the reduced N_5-adducts (**2**, blue; **3**, green; **4**, orange; **5**, red) studied here, in aqueous solution (**5** in a 50/50 % vol. water-acetonitrile mixture), compared to the spectrum of $FADH^-$ in the same conditions (**1**, blue; reproduced from Ref. [34]). While the spectrum of **1** is very weakly structured between 280 and 500 nm, the spectra of the adducts

[†] The transitions T_i (an allowed transition from the ground singlet state S_0 to an excited singlet state) in this paper are the same that have been previously described in Ref 34. This notation does not imply anything about the nature of the state reached by this transition.

display much clearer structures. **2**, **3** and **5** exhibit fully developed bands peaking at 332, 371 and 372 nm, respectively, whereas **4** shows a marked shoulder around 350 nm (and another one around 310 nm). It thus appears that the N_5 substitutions reported here induce a strong loss of absorbance above ~425 nm and above ~385 nm for **2**.

We finally mention that the steady-state fluorescence of **2**, **3**, **4** and **5** was too weak to be recorded satisfactorily (mostly because of a spurious fluorescence background coming from traces of oxidized FAD). However the fluorescence spectrum of **3O**, structurally related to **3**, is significantly more intense and has been reported by Hamdane *et al*.[77] It shows a maximum at 459 nm, upon excitation at 350 nm. This is relatively similar to the fluorescence spectrum of **1** in aqueous solution reported by Kao *et al.*,[8] which peaks around 430 nm (the fluorescence maximum in fact shifts from ~410 to ~450 nm as the excitation was tuned from 320 to 370 nm). It may also be recalled that the fluorescence of reduced tetraacetyl riboflavin in ethanol at 77 K was reported to peak at 515 nm,[6] and was found to be the mirror image of the lowest-energy absorption transition (T_1, peaking at 415 nm in this case).

Note that the traces of FAD_{ox} in our samples could be observed by fluorescence spectroscopy because its excited-state lifetime (in extended form) is rather long (~3 ns[32]), hence its fluorescence quantum yield is much larger than the ones of our reduced flavins. It remains that the absolute amount of FAD_{ox} in our samples is minute and its contribution to absorption spectroscopy is expected to be negligible.

3.2. Transient absorption spectroscopy

3.2.1. Common features

We performed femtosecond transient absorption spectroscopy of the reduced N_5-adducts (**2**, **3**, **4** and **5**) in aqueous solution (50/50 % vol. water-acetonitrile for **5**) with excitation at 360 nm. Some typical transient spectra are shown in Fig. 3, at selected pump-probe delays within a time window of 3.2 ns. Transient spectra of **1**, as published by Dozova *et al*.,[34] are reproduced for reference in ESI,† Fig. S1A.

The transient spectra presented here display significant variations between systems but some common features, already found in **1**,[34] may be highlighted. Most spectra show a positive band at around 400 nm (named TA_1), with more or less marked substructures; TA_1 appears somewhat red-shifted to ~425 nm in **5**. Another broad positive band appears above 500 nm, with larger intensity. For convenience, we will name it TA_2 when its maximum peaks around 500 nm and TA_3 when it peaks further in the red (typically around or above 600 nm) or appears as a distinct shoulder on the red side of a TA_2 band. All spectra are essentially positive over the presented spectral range, indicating that

the expected negative bleaching and stimulated emission contributions are not dominant. The bleaching contributions appear as more or less marked dips below 400 nm. Stimulated emission contributions appear as dips between ~420 and ~450 nm, in qualitative agreement with the indirect information available on the fluorescence of those compounds, as discussed in Section 3.1. We expect the oscillator strength of this emission transition to be of the same order of magnitude as the one of the lowest absorption transition, which is allowed (see ESI,† Table S11). The absence of experimental fluorescence is essentially due to the very short lifetime of the excited state (see below). Contamination by the fluorescence of traces of FAD_{ox} also explains why we could not detect the very weak fluorescence of our adducts (see Section 3.1).

We used multiexponential global analysis (see Section 2.2) to characterize the time evolution of the transient spectra. The results are gathered in Table 1 (time constants); the corresponding DADS and EADS are provided for reference in ESI,† Fig. S4 and Fig. S5. For convenience, the EADS are also presented in normalized form in ESI,† Fig. S6. The EADS of **1**, taken from Ref. [34], are recalled in ESI,† Fig. S1B. To characterize the overall excited-state decay, we integrated the transient spectra between 380 and 700 nm, in order to smooth out the spectral changes occurring while the transient population evolves on the excited-state surface. The obtained kinetic traces (ESI,† Fig. S7) were then fitted to sum of exponentials (parameters in Table 2). The average decay time ($\overline{\tau}$) and standard deviation of decay times (σ) were finally calculated (values in Table 3) using the fitted parameters, as detailed in Ref. [34].

*3.2.2. Compound **3** (methyl thioester)*

We start with compound **3** as its transient spectra are relatively close to those of **1**. Let us recall that **1** initially shows a broad TA_2 band with a week TA_3 shoulder on its red side (see ESI, † Section S1). The TA_3 shoulder disappears in a couple ps and excited-state decay follows in a few tens of ps. Compound **3** is characterized by a much clearer and more intense TA_3 band, peaking at ~583 nm, while the TA_2 band only appear as a shoulder around 500 nm (see for instance EADS1 in Fig. S5-**3**). The TA_3 band of **3** is then seen to rapidly shift to the blue while the TA_2 shoulder grows (see EADS2), with a time constant of 0.61 ps. This evolution proceeds further in 2.8 ps with the full disappearance of the TA_3 band, leaving a relatively narrow TA_2 band peaking at 513 nm (see EADS3). This two-step phenomenon is in fact likely the continuous evolution mentioned in the Introduction, artificially captured as a biexponential process by the global analysis procedure. It is quite evocative of a similar evolution reported earlier for **1** in aqueous solution,[34] albeit with a larger spectral amplitude. In both cases, a band narrowing takes place in a few ps, leaving nearly the same TA_2 maximum at around 515 nm. Some excited-state decay may occur during these early steps but most of the ground-state recovery takes place in 10 ps. The average decay times we calculate ($\overline{\tau}$ in Table 3) is 15 ps (vs. 19 ps for **1**).

A small plateau remains after the 10-ps phase (EADS4 in Fig. S5-**3**), the nature of which is not clear. Unlike **1** in solution,[34] it is not straightforward to assign such signal to the biphotonic ionization of the molecule and concomitant production of hydrated electron. It does not either match with any known signature of FAD_{ox} in solution.[32] It might have arisen from experimental artifacts and will be ignored in the following.

*3.2.3. Compound **2** (carbinolamine)*

The case of compound **2** is significantly different from **1** and **3**. It may first be noted that the transient spectrum at early time does not show any significant TA_2 band around 500 nm (Fig. 3-**2**). Instead, an intense TA_3 band is seen, peaking at ~615 nm (extrapolated at ~630 nm at t=0 in EADS1, Fig. S5-**2**). This band rapidly shifts to the blue in 0.37 and 1.1 ps, while already losing some intensity. Most of the decay then follows in 2.2 ps. It may be observed that the spectrum remaining after the 2.2 ps phase (EADS4) is considerably blue shifted, with a TA_2 maximum at around 510 nm (see NEADS4 in Fig. S6-**2**). The overall blue shift while decaying is a continuous process, as is well seen with the normalized transient absorption spectra (Fig. S3-**2**). The last step of decay occurs in 29 ps. The average decay time of **2** is 11 ps. It is the shortest one of the whole series of compounds we have studied, including **1**.

*3.2.4. Compound **4** (nitrile thioester)*

The transient absorption spectra of **4** (Fig. 3-**4**) bear resemblances with those of **3** and **2** but is characterized by unique aspects. The initial transient spectrum shows a large TA_3 band as for **2** but it is extremely red-shifted, with a maximum at ~660 nm, and it is not dominant. The initial spectrum also displays a substantial TA_2 band, which is on the contrary very blue-shifted, with a maximum at ~470 nm. A clear minimum between TA_2 and TA_3 bands appear around 550 nm. This unusual initial spectrum rapidly evolves, in 1.5 ps (Fig. S5-**4**), by losing its TA_3 component and building a familiar TA_2 maximum at ~500 nm. The initial relaxation happens here without major loss of transient absorbance, hence likely without any substantial loss of excited population, like in **3** but contrary to **2**. The following excited-state multiexponential decay occurs with only some minor narrowing of the TA_2 band; it is globally characterized by an average decay time of 85 ps, which is significantly longer than the corresponding ones of **3** (15 ps) and **2** (11 ps).

*3.2.5. Compound **5** (phenyl thioester)*

The last compound of our series, **5**, has the simplest transient absorption spectra. From the beginning to the end of the evolution, one observes a dominant TA_2 band located around 510 nm. It is in fact seen to slightly blue shift with time, from ~513 nm at early times to ~498 nm towards the end of the decay (Fig. 3-**5** and Fig. S3-**5**). A shapeless red wing is also present at all times and does not qualify as a *bona fide* TA_3 band. The blue shift of the TA_2 band is seen to start without major loss of

excited population with a time constant of 0.31 ps but is also seen to continue during the following excited-state decay steps, in 5.9, 35 and 184 ps. The average excited-state decay time of **5** is 78 ps.

3.3. Theoretical calculations

It is well known that the substituent on N_{10} in FAD does not participate in the conjugated system and does not modify the absorption spectrum of the flavin[78,79]. Therefore it is usual to use lumiflavins as models for studying more complex flavins in order to reduce the number of degrees of freedom for theoretical calculations. Because our explicit solvent model is very demanding in time and computational resources we chose to study theoretically only three lumiflavins (**1'**, **2'** and **3')** because their FAD equivalents (reduced flavin **1** and substituted flavins **2** and **3**, which mimics the adduct **3O**) have already been experimentally observed in proteins.[61,77]

3.3.1. Ground-state geometries

The geometries of the most stable isomers of the three lumiflavin derivatives (**1'**, **2'** and **3'**) in water were optimized with both PBE1PBE and CAM-B3LYP functionals, using implicit solvation (PCM) and explicit solvation (following the procedure described in Section 2.3).

Both functionals with both solvation models yielded essentially the same geometries (shown in Fig. 4A with PBE1PBE) for all compounds. All structures and their Cartesian coordinates are provided in ESI,† Section S3.1.

As expected, the three lumiflavin derivatives are not planar but bent along the N_5-N_{10} axis. The dihedral angle ϕ (cf. ESI,† Section S3.1) between the two cycles has been chosen to measure this bend and is also shown in Fig. 4A. It is interesting to notice that **2'** exhibits an intramolecular H-bond between the OH group and the carbonyl at C_4, while in **3'** the S-CH_3 group is folded on top of the re-face of the isoalloxazine ring with the methyl group oriented above the phenyl ring.

As compared to the PCM model, the explicit treatment of water molecules leads to even more similar structures calculated by the two functionals and accentuates the differences between the three derivatives: for **1'** angle ϕ is 26°; it increases to 36° for **2'** and decreases to 13° for **3'**.

3.3.2. UV-visible spectra

TDDFT calculations were performed on the optimized structures, with both functionals and both solvation models, to obtain the steady state UV-visible spectra of the three adducts. The PBE1PBE spectra calculated with explicit and implicit water models are shown in Fig. 5. CAM-B3LYP spectra are very similar, except for an overall blue shift and are reported in Fig. S11.

As expected from the literature (see Section 3.1), the shape of these spectra between *ca.* 280 and 500 nm essentially results from the overlap of three allowed transitions (T_1, T_2 and T_3, from red to blue) and is governed by their relative shifts and intensities. The positions of both T_1 and T_2

transitions are influenced by the nature of the substituents on N_5, while the position of the T_3 transition remains mostly unchanged in all molecules. The wavelengths of the three transitions for PBE1PBE and CAM-B3LYP with explicit and implicit water models are gathered in ESI,† Tables S7 and S8, respectively.

Fig. 5 clearly shows that the PCM model is unable to correctly reproduce the experimental spectra, which seems to come from a poor description of the T_1 and T_2 transitions (Fig. 5 and Table S7). On the other hand, explicit consideration of water molecules leads to a good reproduction of the spectra (see discussion in Section 4.1). Consequently, the rest of the analysis will only focus on the explicit treatment of water molecules with the PBE1PBE/6-311++g(d,p) level of theory. Results with the other methods are however gathered in ESI,† Section S3.3.

The analysis of the transition associated with an excited state by TDDFT is not always straightforward. This transition may be a combination of several orbital transitions with similar coefficients. The use of Natural Transition Orbitals (NTO)[80] provides a more intuitive picture of the hole–particle excitation by transforming the ordinary orbital representation into a form in which each excited state is expressed as a single pair of orbitals. In order to compare the calculated allowed transitions in the three lumiflavins we used NTO analysis which is especially useful for delocalized chromophores. Each transition T_n (n=1, 2 or 3) can be represented by the excitation of one electron from the NTO particle orbital P_n to the corresponding allowed NTO hole orbital H_n. For the three lumiflavin analogues studied here, the calculations show that the particle orbitals P_1, P_2 and P_3 are always identical to the HOMO of the corresponding lumiflavin molecule. Consequently, only P_1 is reported for **1'**, **2'** and **3'** in ESI,† Fig. S12, together with H_1, H_2 and H_3 orbitals, for the PBE1PBE calculations with explicit solvation. The NTOs obtained with other methods are gathered in Fig. S13-S15.

The analysis of these orbitals leads to the following conclusions:

- P_1 (and thus P_2 and P_3) is a π orbital delocalized over all the isoalloxazine, very similar for the three adducts;
- H_1 is a π^* orbital delocalized over all the cycles of the molecules, identical for the three adducts;
- H_2 is a π^* orbital localized on the phenyl ring of the isoalloxazine chromophore and very similar for the three adducts;
- H_3 is a π^* orbital mainly localized on the uracyl ring of the isoalloxazine chromophore, with a weak participation of the phenyl ring for **1'** and **2'**;
- N_5 is never involved in H_1 and H_2 orbitals while it is highly involved in P_1 (and P_2), for all adducts;
- No water molecules are involved in these orbitals.

The energy diagram of the transitions for **1'**, **2'** and **3'** is shown in Fig. S16. As the particle orbitals P_1, P_2 and P_3 are strictly identical to the HOMO of each lumiflavin, we used the HOMO energies for the particle orbitals to build the diagram. The hole orbitals energies were estimated by adding the energy of each transition to the energy of the corresponding particle orbital.

For the T_1 transition, both P_1 and H_1 energy levels of **2'** and **3'** decrease as compared to **1'**, but it is mainly the energy differences between P_1 orbitals and consequently between the HOMOs which explain the energy differences of the three T_1 transitions. This observation is much more obvious in the case of transition T_2, since the energy levels of H_2 are almost identical between the three systems: only the energy differences between the HOMOs of each analog explain the energy differences between the three T_2 transitions. T_3 transitions are similar in energy for the three lumiflavin because the energy levels of the P_3 and H_3 decrease in the same proportions when going from **1'** to **2'** and **3'**.

3.3.3. First excited-state geometries

Transient absorption spectroscopy experiments were done with excitation at 360 nm. This corresponds to the T_1 transition region for **1'**, **2'** and **3'**. Therefore, we have also optimized the structure of the first excited state (ES_1) corresponding to this transition with TDDFT, using the functional which best reproduces steady state UV-visible spectra, namely PBE1PBE/6-311++g(d,p), with both the explicit solvation and PCM model. Optimized excited state geometries with both methods are in good agreement: the angles ϕ are compiled in Table S1 and the geometries for the explicit model are reported in Fig. 4B. Water molecules have been masked to make reading easier. The vertical absorption and fluorescence energies between the ground state and the first excited state are given in ESI,† (Table S11), together with the associated oscillator strengths and transition electric dipole moments, and the adiabatic energies for **1'**, **2'** and **3'**.

Compared to ground-state structures, the bending angle ϕ is reduced in the exited state. **1'** becomes almost planar (2.9° with the explicit model) and the angles of both **2'** and **3'** both decrease (to 10.4° and 9.5°, respectively). In addition to their remaining ϕ fold, the latter two adducts exhibit another deviation from planarity as the phenyl ring twists with respect to the uracyl ring (along the long axis of the molecule). This is most likely due to steric effects (for both **2'** and **3'**) and to the intramolecular hydrogen bond between the hydrogen of the alcohol and the oxygen of the C_4 carbonyl in the case of **2'**.

4. DISCUSSION

4.1. Implicit versus explicit treatment of water molecules to study lumiflavin derivatives

The goal of this theoretical study was to understand the shifts in the steady-state UV-visible spectra of the three lumiflavin molecules. The two functionals that we used, PBE1PBE and CAM-B3LYP have already given good results for TDDFT calculations in solution.[81] As mentioned before, both PBE1PBE and CAM-B3LYP yield comparable results for **1'**, **2'** and **3'**, but CAM-B3LYP exhibits a marked blue shift as compared to the experimental data (cf. Fig. S11). Therefore, we will mainly discuss PBE1PBE results in this section. We were only interested in the first three allowed transitions T_1, T_2 and T_3 which are at the origin of the experimentally observed spectra.

Let us here recall that Ghisla *et al.*[82] proposed that transition T_1 depends highly on the degree of planarity of the isoalloxazine ring. Experimentally, tetragonalization of N_5 (*e.g.* protonation) abolishes this transition, while simple substitution at N_5 shifts it to the blue. It was in particular observed that the maximum of transition T_1 is hypsochromically shifted up to 30 nm in a series of adducts with increasing size of the alkyl substituent in N_5. Ghisla *et al.*[82] proposed that this shift results from an increasingly bent conformation of the isoalloxazine and further argued[6] that alkyl substitution in N_5 results in a single, structureless absorption band, centered around 325-350 nm, consisting of two unresolved transitions, T_1 and T_2.

We first attempted to take into account water solvation by an implicit solvation model, namely PCM. As seen in Fig. 5 (left), this method demonstrates well that the spectra (down to ~265 nm) arise from the overlap of three transitions and reproduces correctly the blue shift of the spectra of **2'** and **3'** with respect to the broad diffuse band of **1'**. These results imply that the well-defined bands in **2'** and **3'** arise from the overlap of the two T_1 and T_2 transitions, as proposed by Ghisla *et al*.[6] However, the calculated spectra differ too much from the experimental ones. The calculated spectrum of **1'** displays a distinct maximum around 335 nm (due to the transition T_2) while the experimental spectrum is essentially shapeless in this region. The calculated spectrum of **2'** only shows a broad shoulder arising from the T_2 transition instead of a well-defined band. Finally, the blue shift of **3'** is of the same magnitude as that of **2'**; the distance between the maxima of absorption bands of these two compounds ($\Delta\lambda_{3'2'} = \lambda_{3'} - \lambda_{2'}$, measured as the distance between the T_2 transitions, mostly responsible for the maxima) is found to be ~8 nm in the simulated spectra, which contradicts the experimental value of 43 nm. These differences thus do not allow any in-depth analysis of the calculations at this level in order to explain the spectral differences between the three molecules.

In order to improve our simulations, we decided to implement the explicit solvation shell with a large number of water molecules to obtain the first solvation layer around the lumiflavin and take into account hydrogen bonds formed between lumiflavin and water or the steric hindrance by the

substituent (both in **2'** and **3'**). The limitation of this approach (described in Section 2.3) is that we focus on a single structure for each system, one snapshoot of the organization hydrated complex. A more rigorous approach would require carrying out many other snapshots and averaging the results, but the cost would be well beyond our calculation capacities. Even though we will use these snapshots to comment on the observed spectral shifts, we are fully aware that other less stable geometries and solvent distributions around the molecule will contribute to the spectra, especially for the substituted adducts where the CH_2-OH and CH_2-S-CH_3 chains are a lot more flexible than the isoalloxazine.

Nevertheless, our single snapshot approach improved significantly the agreement between experiment and calculation, as shown in Fig. 5 (right). The relative intensities of the three transitions in **1'** are in better accordance with the experimental spectrum. The absorption band of **2'** is now clearly defined, and the spectral distance between **2'** and **3'** increases ($\Delta\lambda_{3'2'}$ = 18 nm). The origin of the blue shift of the absorption band here is partly due to a large blue shift of transition T_2 (in **2'** and **3'** as compared to **1'**) which frees the 300-400 nm region. The band observed in this region for **2'** and **3'** is thus exclusively due to the T_1 transition. It should also be noted that the spectral position of the T_1 transition shifts to the blue upon substitution, as follows: $\lambda_{1'}(T_1) > \lambda_{3'}(T_1) > \lambda_{2'}(T_1)$ (Fig. 5 (right)). This explains why the absorption spectra of **2'** and **3'** become both blue shifted and better defined than that of **1'**. The three transitions of **1'**, more of less evenly spaced in energy, indeed tend to strongly overlap and produce a shapeless absorption continuum. Conversely, the larger separation between transition T_1 and the group of transitions T_2 and T_3 produces a much more structured absorption spectrum in **2'** and **3'**.

The above results show that the origin of the experimentally observed band is highly sensitive to the method used for the calculation and that the choice of the best method is not straightforward. Since the explicit solvation calculations reproduce the experimental data far better that those using the PCM model, we will discuss exclusively the former, with the PBE1PBE/6-311++g(d,p) functional, in the following.

Let us also highlight that our results formally contradict Ghisla's interpretative framework according to which the hypsochromically shifted lowest absorption band of N_5-subtituted flavins (**2'** and **3'**) arises from nearly degenerate T_1 and T_2 transitions. Our findings on the contrary assign it to the T_1 transition only, T_2 shifting even more to the blue and getting in fact pretty close to transition T_3 (the shift of which is rather small).

4.2. Origin of the observed blue shift in UV-visible stationary spectra

Within Ghisla's framework, the blue shift of the absorption spectrum upon N_5 substitution is attributed to an increase of the bend angle along the N_5-N_{10} axis, as compared to **1**. Comparison of

the dihedral angles of our lumiflavin compounds in the presence of an explicit hydration shell shows a different trend. The bend angle of the isoalloxazine ring (ϕ) was found to be 26.5° for **1'**, 36.4° for **2'** and 13.3° for **3'** (cf. Fig. 4A and Table S1). Our value for **1'** is in good agreement with previously reported value[17,19,23] and ϕ is indeed found to be larger for **2'**, in agreement with Ghisla's guideline. It however turns out that ϕ is significantly lower for **3'**, which disagrees with this guideline. In other words, our theoretical calculations show that **3'** is more planar than **1'** even though its spectrum is blue shifted in respect to the spectrum of the unsubstituted lumiflavin. This important finding definitely contradicts the interpretation that the bend angle is the key determinant for determining the blue shift of the absorption spectrum.

The analysis of the NTOs (Fig. S12 and Section 3.3.2) clearly shows that the P_1, H_1 and H_2 orbitals are identical for **1'**, **2'** and **3'** and that H_3's are very similar. So, from an orbital point of view, whatever the substituent on N_5, the nature of the T_1, T_2 and T_3 transitions does not change. On the other hand, the energy diagram of the transitions (ESI,† Fig. S16) shows that the energy of the particle orbital P_1 (*i.e.* the energy of the HOMO) of the three molecules is strongly lowered upon N_5 substitution, while the corresponding hole orbitals undergo a more limited stabilization. This phenomenon is mainly responsible for the blue shifts of the T_1 and T_2 transitions and, as the NTOs show, correlates with the fact that the N_5 atom is involved in P_1 for the three systems but never in their H_1 or H_2 orbitals. As far as the T_3 transition is concerned, the P_3 and H_3 energy levels shift by approximately the same amount upon substitution, which leads to similar transition energies for the three molecules.

The question arises then as to whether the N_5-substituent-dependent change in HOMO energy is mainly due to the electronic nature of the substituent, or rather to a different organization of the water molecules around the lumiflavins, induced by the change in substituent. We therefore recalculated the HOMO energy of the three lumiflavins in the geometry obtained with the explicit solvent treatment, but without the water molecules. These are shown in Table S9, together with the HOMO energies obtained in the presence of water molecules. Taking **1'** as a reference, the HOMO energy drops by -0.53 eV for **2'** and -0.44 eV for **3'** in the presence of water molecules and by -0.40 eV and -0.34 eV without them. It is thus mainly the change of adduct in N_5 which governs the gap between the HOMO energies of the three lumiflavins. Water molecules accentuate this effect but in smaller proportions.

To try to better understand the differences in behavior between the three systems, we have also analyzed atomic charges, summed per fragment of the molecule in Table S10. Two different approaches were used to compute charges: Bader charges, obtained by atomic partitioning of the electron density, and NPA charges (natural population analysis) obtained by an orbital approach to partitioning natural orbitals. The objective is not to discuss the distribution of charges, the two

methods leading to different partitioning, but to see if we observe a different behavior by changing the adduct in N_5.

Both methods lead to the same conclusion: no notable variation is observed between **1'**, **2'** and **3'**. This means that neither the electron density (Bader charges) nor the natural orbitals (NPA charges) of each fragment are notably affected by the N_5 substitution. We however note that the total charge of the molecules is not exactly -1 (-0.9 for NPA charges and -0.7 for Bader charges) indicating that part of the charge is carried by the network of water molecules. This could explain why the implicit treatment of water molecules by PCM is not sufficient to correctly model these negatively charged systems.

Finally, we conclude that the main reason for the blue shift of the T_1 and T_2 transitions, and thus for the observed well defined bands of **2'** and **3'** as compared to the unstructured **1'** spectrum, is the stabilization of the HOMO orbital upon substitution of the hydrogen atom by a CH_2-OH or CH_2-S-CH_3 group. Other factors like the shape of the Natural Transition Orbitals of the three transitions or atomic charges are too similar for all three molecules to account for the spectra difference, while the shift of the bands from **1'** to **3'** to **2'** is not consistent with the corresponding calculated bend angles.

4.3. Evolution on the excited-state surface

To interpret the transient absorption data, we globally apply the framework recalled in the Introduction and used in Ref.[34] It consists in relating the evolution of the transient spectra to the motion of the excited-state population along some large-amplitude coordinate, loosely identified as the butterfly bending coordinate. This motion is supposed to lead to a conical intersection (CI) with the ground state where the excited population rapidly deactivates. Within this point of view, the spectral changes during the evolution on the excited-state surface are fundamentally continuous but are transcribed within experimental noise into a discrete sum of exponentials by our global analysis approach. A sense of the continuous nature of the excited-state evolution may be got by inspecting the raw transient spectra, normalized at the maximum of the TA_2/TA_3 band (Fig. S3).

The fastest steps of evolution of the transient absorption spectra, occurring in the sub-ps regime (except 1.5 ps for **4**; see τ_1 in Table 1), may in fact contain contributions from the dielectric response of the immediate surroundings, driven by the change of charge distribution upon excitation. Solvation dynamics is indeed known to be extremely fast for water, with a large part of it taking place in the sub-ps regime.[83,84] It is also not excluded that traces of internal conversion between excited states, from the initially excited state at the current excitation wavelength to the lowest-lying excited state, might also contribute in that timescale,[23] although such phenomenon is expected to be extremely fast (possibly in the 100-fs timescale) given that the small energy separation between

them (energy gap law[85]). We however propose that these earliest kinetic steps are dominated by the beginning of the evolution on the excited-state mentioned above.

It is interesting at this level to mention that our theoretical calculations (performed with the PCM and explicit solvation methods) show that the optimized geometry of the lowest excited state (ES_1) of all examined lumiflavin analogs (**1'**, **2'**, **3'**) tends to be more planar than the ground state (see Section 3.3.3). In the case of **1'** the planarity is almost perfect, while in the case of the two adducts steric affects and the intermolecular H bond (in **2'**) prevent the complete planarization of the excited state which retains a smaller fold angle and some twist along the long axis of the molecule (Fig. 4B). This result suggests that the excited state initially produced by the ultrashort excitation of our setup, which is expected to bear the bent configuration of the ground state, would tend to relax its geometry towards a more planar structure. Let us note that this planarization might be only partial if the CI to the ground state is encountered in the way. This dynamic trend should however constitute a common feature of all compounds studied in this work, including **1**.

It is worth recalling that during the initial steps of the excited-state evolution of all compounds, from sub-ps to a few ps, the transient absorption spectrum above ~450 nm undergoes a blue shift and narrowing. The TA_3 structure, seen as a shoulder on the red side of the TA_2 band or as a distinct band around 600 nm, is seen to disappear and leave a narrower TA_2 band centered at around 500 nm (see NEADS in Figs. S2B and S6). This phenomenon is much less marked for **5** but still existing. Assuming that planarization of the isoalloxazine is under way during those steps, we propose that TA_3 bands or shoulders should be characteristic of bent configurations while TA_2 bands would rather sign more planar configurations. In practical terms, it is likely a distribution of bend angles that would determine the exact shape of the transient spectra. It may at this respect be recalled that the isoalloxazine ring is expected to be rather flexible about the butterfly bending; barrier to ring inversion along this coordinate were indeed reported to be low (2-4.8 kcal/mol) for different reduced flavins.[14-16,18] Broad initial distributions, reflecting the configuration of the ground state selected by the excitation, would correspond to broad spectra with TA_2 and TA_3 contributions, while relaxed distributions, hypothetically more centered about a more planar configuration, would give rise to narrower spectra, restricted to a dominant TA_2 contribution. The case of **5** appears more difficult to accommodate within that view since it does not show much of a clear TA_3 contribution at short times and very little spectral narrowing over the transient dynamics. It might be tentatively proposed that the initial, ground-state-inherited, configuration of **5** is rather planar, more so than compounds **1**-**4**, but we do not have so far any theoretical element supporting this hypothesis. Alternatively, it could be argued that the shapeless background observed beyond 600 nm is a kind of extremely wide and red-shifted TA_3 structure, still reflecting bend configurations. The fact that this structure never

disappears would suggest that planarization would be hindered for these particular configurations of **5**. Additional theoretical calculations would be necessary to establish a reliable interpretation.

4.4. Excited-state decay

As far as the decay of the excited state is concerned, it is interesting to note that, for compounds **1**, **3** and **4**, the excited-state decays mostly take place after the shift and narrowing process is completed (see Fig. S1B and Fig. S5). This suggests that the CI to the ground state is not located close to the initial conformation of the molecule and that some structural relaxation, hypothetically planarization, is required before it can be reached. It may additionally be observed that the average excited-state lifetime ($\overline{\tau}$, Table 3) of **1** and **3** is rather short (19 and 15 ps, respectively) while it is much longer for **4** (85 ps). This suggests that the CI of **4** could be located farther away from both the initial and relaxed configurations of the excited state than in the case of **1** or **3**. Alternatively, it is not excluded that, for some unknown reason, the rigidity of the isoalloxazine ring of **4** would be larger than that of **1** and **3**, hence justifying the slower excited-state dynamics of this compound.

The case of **2** is quite interesting as one observes a strong loss of transient absorption signal during the red shifting of the TA_3 band. This is interpreted as a strong excited-state decay taking place while the excited state structurally relaxes – possibly towards a more planar configuration. This in turn suggests that the CI to the ground state of **2** probably lies closer to the initial bent configuration than in **1**, **3** or **4**. This might be convergent with the fact that the calculated geometry for the first excited state of **2'** is less planar than those of **1'** and **3'**.

As mentioned above, the case of **5** is comparatively harder to interpret. It should however be noted that the average excited-state lifetime of **5** is quite long (78 ps), suggesting as for **4** that the CI to the ground state is not located close to the initial nor the relaxed configuration. The possibility that the structure of this compound is somewhat more rigid than that of **1**, **3** or **4** should also not be discarded.

Overall, the differences of excited-state lifetime observed across the **1**-**5** series point to the fact that the position, *i.e.* the geometry of the CI would significantly depend on the nature of the N_5 substitution.

5. CONCLUSIONS

In this study, we explored the steady-state and transient absorption spectroscopy of several N_5-substitued derivatives of $FADH^-$ (**2**, **3**, **4**, **5**; Fig. 1) in aqueous solution, guided by DFT/TDDFT calculations for interpretation. While implicit solvation (PCM) reproduces well the geometry of the

different molecules, explicit treatment of water molecules is necessary for correctly modeling steady-state spectra. Unlike the nearly unstructured steady-state absorption spectrum of $FADH^-$ (**1**), most N_5-adducts studied here display a well-structured absorption spectrum, with a marked absorption band around 330 nm (**2**) or 370 nm (**3**, **5**; shoulder for **4**) and a loss of absorbance above 425 nm. Contrary to previous interpretations linking these changes to an increased bend angle of the isoalloxazine ring along the N_5-N_{10} axis, our explicit solvent calculations suggest that the bend angle plays a minor role. Instead, the observed blue shift and structured spectra arise from HOMO stabilization in N_5-substituted adducts, which shifts and separates the T_1 and T_2 transitions.

Transient absorption spectra reveal both similarities and significant differences among the compounds. Above ~450 nm, we identify two key transient absorption bands: TA_2 (~500 nm) and TA_3 (~600 nm, seen as a red-side shoulder or independent band). Initially, combinations of TA_2 and TA_3 appear, but spectra stabilize within picoseconds, dominated by a narrow TA_2 band. Computational results indicate that while the excited state of **1'** is planar, steric and hydrogen-bonding effects in **2'** and **3'** prevent planarity, retaining a dihedral angle and twist. Across all molecules, relaxation to the lowest-lying excited state involves decreased bending of the isoalloxazine ring compared to the ground state, suggesting that TA_2 reflects more planar geometries, whereas TA_3 signifies bent configurations inherited from the ground state. It may be kept in mind that this hypothesized planarization process is simply a relaxation of the dihedral angle along the butterfly coordinate.

The ultrafast decay of the excited state (11 to 85 ps; see Table 1) likely occurs via conical intersections (CIs) along the relaxation pathway. The fastest decays (**1**, **2**, **3**) likely sign situations where the CI is located near the initial configuration. This should be particularly true of **2**, for which the excited-state decay starts before the spectral/structural relaxation even begins. Conversely the slowest decays (**4**, **5**) probably correspond to geometries of the CI situated both farther away for the initial or the relaxed configurations than in **1**-**3**. Our results globally suggest that the position of the CI would significantly depend on the nature of the N_5 substituent. We were not able to rationalize this effect in terms of structural parameters but we stress that the excited-state lifetime is likely controlled in part by the position of the CI.

While steady-state spectra of the three thio substituted adducts (**3-5)** are very similar because of the probable equivalent stabilization of the HOMO orbital, their transient absorption spectra and their decays exhibit different behavior indicating that other factors depending on the interaction of the different N_5 substituents with the molecule and/or the solvent might influence the evolution of the excited state and the position of the CI. Further theoretical investigations would be required to understand better this phenomenon. Our findings underscore the intricate photophysical behavior of anionic reduced flavins under peripheral N_5 substitution and provide a foundation for future investigations of other reduced flavin derivatives.

CONFLICT OF INTERESTS

There are no conflicts to declare.

ACKNOWLEDGEMENTS

REFERENCES

(1) Ghisla, S.; Massey, V. Mechanisms of Flavoprotein-Catalyzed Reactions. *Eur. J. Biochem.* **1989**, *181*, 1-17.
(2) Walsh, C. T.; Wencewicz, T. A. Flavoenzymes: Versatile Catalysts in Biosynthetic Pathways. *Nat. Prod. Rep.* **2013**, *30*, 175-200.
(3) Leys, D.; Scrutton, N. S. Sweating the Assets of Flavin Cofactors: New Insight of Chemical Versatility from Knowledge of Structure and Mechanism. *Curr. Opin. Struct. Biol.* **2016**, *41*, 19-26.
(4) Piano, V.; Palfey, B. A.; Mattevi, A. Flavins as Covalent Catalysts: New Mechanisms Emerge. *Trends Biochem. Sci.* **2017**, *42*, 457-469.
(5) Lombard, M.; Hamdane, D. Flavin-Dependent Epitranscriptomic World. *Arch. Biochem. Biophys.* **2017**, *632*, 28-40.
(6) Ghisla, S.; Massey, V.; Lhoste, J. M.; Mayhew, S. G. Fluorescence and Optical Characteristics of Reduced Flavines and Flavoproteins. *Biochemistry* **1974**, *13*, 589-597.
(7) Li, G. F.; Glusac, K. D. Light-Triggered Proton and Electron Transfer in Flavin Cofactors. *J. Phys. Chem. A* **2008**, *112*, 4573-4583.
(8) Kao, Y. T.; Saxena, C.; He, T. F.; Guo, L. J.; Wang, L. J.; Sancar, A.; Zhong, D. P. Ultrafast Dynamics of Flavins in Five Redox States. *J. Am. Chem. Soc.* **2008**, *130*, 13132-13139.
(9) Galban, J.; Sanz-Vicente, I.; Navarro, J.; de Marcos, S. The Intrinsic Fluorescence of FAD and Its Application in Analytical Chemistry: A Review. *Methods Appl. Fluoresc.* **2016**, *4*, 19.
(10) Losi, A. Flavin-Based Blue-Light Photosensors: A Photobiophysics Update. *Photochem. Photobiol.* **2007**, *83*, 1283-1300.
(11) Sancar, A. Structure and Function of DNA Photolyase and Cryptochrome Blue-Light Photoreceptors. *Chem. Rev.* **2003**, *103*, 2203-2237.
(12) Sorigué, D.; Hadjidemetriou, K.; Blangy, S.; Gotthard, G.; Bonvalet, A.; Coquelle, N.; Samire, P.; Aleksandrov, A.; Antonucci, L.; Benachir, A. et al. Mechanism and Dynamics of Fatty Acid Photodecarboxylase. *Science* **2021**, *372*, eabd5687.
(13) Moonen, C. T. W.; Vervoort, J.; Muller, F. Reinvestigation of the Structure of Oxidized and Reduced Flavin: Carbon-13 and Nitrogen-15 Nuclear Magnetic Resonance Study. *Biochemistry* **1984**, *23*, 4859-4867.
(14) Moonen, C. T. W.; Vervoort, J.; Muller, F. Carbon-13 Nuclear Magnetic Resonance Study on the Dynamics of the Conformation of Reduced Flavin. *Biochemistry* **1984**, *23*, 4868-4872.
(15) Dixon, D. A.; Lindner, D. L.; Branchaud, B.; Lipscomb, W. N. Conformations and Electronic Structures of Oxidized and Reduced Isoalloxazine. *Biochemistry* **1979**, *18*, 5770-5775.
(16) Hall, L. H.; Bowers, M. L.; Durfor, C. N. Further Consideration of Flavin Coenzyme Biochemistry Afforded by Geometry-Optimized Molecular-Orbital Calculations. *Biochemistry* **1987**, *26*, 7401-7409.

(17) Meyer, M.; Hartwig, H.; Schomburg, D. Semiempirical and Ab Initio Study of Closed and Open Shell Derivatives of 10-Methylisoalloxazine: A Model of Flavin Redox States. *J. Mol. Struct. (Theochem)* **1996**, *364*, 139-149.
(18) Zheng, Y.-J.; Ornstein, R. L. A Theoretical Study of the Structures of Flavin in Different Oxidation and Protonation States. *J. Am. Chem. Soc.* **1996**, *118*, 9402-9408.
(19) Hahn, J.; Michel-Beyerle, M. E.; Rosch, N. Conformation of the Flavin Adenine Dinucleotide Cofactor FAD in DNA-Photolyase: A Molecular Dynamics Study. *J. Mol. Model.* **1998**, *4*, 73-82.
(20) Rizzo, C. J. Further Computational Studies on the Conformation of 1,5-Dihydrolumiflavin. *Antioxid. Redox Signal.* **2001**, *3*, 737-746.
(21) Rodríguez-Otero, J.; Martínez-Núñez, E.; Peña-Gallego, A.; Vázquez, S. A. The Role of Aromaticity in the Planarity of Lumiflavin. *The Journal of Organic Chemistry* **2002**, *67*, 6347-6352.
(22) Choe, Y.-K.; Nagase, S.; Nishimoto, K. Theoretical Study of the Electronic Spectra of Oxidized and Reduced States of Lumiflavin and Its Derivative. *J. Comput. Chem.* **2007**, *28*, 727-739.
(23) Pauszek, R. F.; Kodali, G.; Siddiqui, M. S. U.; Stanley, R. J. Overlapping Electronic States with Nearly Parallel Transition Dipole Moments in Reduced Anionic Flavin Can Distort Photobiological Dynamics. *J. Am. Chem. Soc.* **2016**, *138*, 14880-14889.
(24) Schwinn, K.; Ferré, N.; Huix-Rotllant, M. UV-Visible Absorption Spectrum of FAD and Its Reduced Forms Embedded in a Cryptochrome Protein. *Phys. Chem. Chem. Phys.* **2020**, *22*, 12447-12455.
(25) Matthews, A.; Saleem-Batcha, R.; Sanders, J. N.; Stull, F.; Houk, K. N.; Teufel, R. Aminoperoxide Adducts Expand the Catalytic Repertoire of Flavin Monooxygenases. *Nature Chemical Biology* **2020**, *16*, 556-563.
(26) Lennon, B. W.; Williams, C. H., Jr.; Ludwig, M. L. Crystal Structure of Reduced Thioredoxin Reductase from *Escherichia Coli*: Structural Flexibility in the Isoalloxazine Ring of the Flavin Adenine Dinucleotide Cofactor. *Protein Sci.* **1999**, *8*, 2366-2379.
(27) Mees, A.; Klar, T.; Gnau, P.; Hennecke, U.; Eker, A. P. M.; Carell, T.; Essen, L. O. Crystal Structure of a Photolyase Bound to a CPD-Like DNA Lesion after in Situ Repair. *Science* **2004**, *306*, 1789-1793.
(28) Dhatwalia, R.; Singh, H.; Oppenheimer, M.; Karr, D. B.; Nix, J. C.; Sobrado, P.; Tanner, J. J. Crystal Structures and Small-Angle X-Ray Scattering Analysis of UDP-Galactopyranose Mutase from the Pathogenic Fungus Aspergillus Fumigatus. *J. Biol. Chem.* **2012**, *287*, 9041-9051.
(29) Enescu, M.; Lindqvist, L.; Soep, B. Excited-State Dynamics of Fully Reduced Flavins and Flavoenzymes Studied at Subpicosecond Time Resolution. *Photochem. Photobiol.* **1998**, *68*, 150-156.
(30) MacFarlane, A. W.; Stanley, R. J. *Cis-Syn* Thymidine Dimer Repair by DNA Photolyase in Real Time. *Biochemistry* **2003**, *42*, 8558-8568.
(31) Li, G. F.; Sichula, V.; Glusac, K. D. Role of Adenine in Thymine-Dimer Repair by Reduced Flavin-Adenine Dinucleotide. *J. Phys. Chem. B* **2008**, *112*, 10758-10764.
(32) Brazard, J.; Usman, A.; Lacombat, F.; Ley, C.; Martin, M. M.; Plaza, P. New Insights into the Ultrafast Photophysics of Oxidized and Reduced FAD in Solution. *J. Phys. Chem. A* **2011**, *115*, 3251-3262.
(33) Zhao, R. K.; Lukacs, A.; Haigney, A.; Brust, R.; Greetham, G. M.; Towrie, M.; Tonge, P. J.; Meech, S. R. Ultrafast Transient Mid IR to Visible Spectroscopy of Fully Reduced Flavins. *Phys. Chem. Chem. Phys.* **2011**, *13*, 17642-17648.
(34) Dozova, N.; Lacombat, F.; Lombard, M.; Hamdane, D.; Plaza, P. Ultrafast Dynamics of Fully Reduced Flavin in Catalytic Structures of Thymidylate Synthase ThyX. *Phys. Chem. Chem. Phys.* **2021**, *23*, 22692-22702.
(35) Visser, A.; Ghisla, S.; Massey, V.; Muller, F.; Veeger, C. Fluorescence Properties of Reduced Flavins and Flavoproteins *Eur. J. Biochem.* **1979**, *101*, 13-21.
(36) Okamura, T.; Sancar, A.; Heelis, P. F.; Begley, T. P.; Hirata, Y.; Mataga, N. Picosecond Laser Photolysis Studies on the Photorepair of Pyrimidine Dimers by DNA Photolyase. 1. Laser

Photolysis of Photolyase-2-Deoxyuridine Dinucleotide Photodimer Complex. *J. Am. Chem. Soc.* **1991**, *113*, 3143-3145.
(37) Leenders, R.; Kooijman, M.; Vanhoek, A.; Veeger, C.; Visser, A. Flavin Dynamics in Reduced Flavodoxins. A Time-Resolved Polarized Fluorescence Study. *Eur. J. Biochem.* **1993**, *211*, 37-45.
(38) Kao, Y. T.; Saxena, C.; Wang, L. J.; Sancar, A.; Zhong, D. P. Direct Observation of Thymine Dimer Repair in DNA by Photolyase. *Proc. Natl. Acad. Sci. USA* **2005**, *102*, 16128-16132.
(39) Kao, Y. T.; Tan, C.; Song, S. H.; Ozturk, N.; Li, J.; Wang, L. J.; Sancar, A.; Zhong, D. P. Ultrafast Dynamics and Anionic Active States of the Flavin Cofactor in Cryptochrome and Photolyase. *J. Am. Chem. Soc.* **2008**, *130*, 7695-7701.
(40) Li, J.; Liu, Z. Y.; Tan, C.; Guo, X. M.; Wang, L. J.; Sancar, A.; Zhong, D. P. Dynamics and Mechanism of Repair of Ultraviolet-Induced (6-4) Photoproduct by Photolyase. *Nature* **2010**, *466*, 887-891.
(41) Thiagarajan, V.; Byrdin, M.; Eker, A. P. M.; Müller, P.; Brettel, K. Kinetics of Cyclobutane Thymine Dimer Splitting by DNA Photolyase Directly Monitored in the UV. *Proc. Natl. Acad. Sci. USA* **2011**, *108*, 9402-9407.
(42) Mathews, II; Deacon, A. M.; Canaves, J. M.; McMullan, D.; Lesley, S. A.; Agarwalla, S.; Kuhn, P. Functional Analysis of Substrate and Cofactor Complex Structures of a Thymidylate Synthase-Complementing Protein. *Structure* **2003**, *11*, 677-690.
(43) Koehn, E. M.; Perissinotti, L. L.; Moghram, S.; Prabhakar, A.; Lesley, S. A.; Mathews, I. I.; Kohen, A. Folate Binding Site of Flavin-Dependent Thymidylate Synthase. *Proc. Natl. Acad. Sci. USA* **2012**, *109*, 15722-15727.
(44) Ai, Y. J.; Zhao, C. F.; Xing, J. L.; Liu, Y.; Wang, Z. X.; Jin, J. R.; Xia, S. H.; Cui, G. L.; Wang, X. K. Excited-State Decay Pathways of Flavin Molecules in Five Redox Forms: The Role of Conical Intersections. *J. Phys. Chem. A* **2018**, *122*, 7954-7961.
(45) Gozem, S.; Mirzakulova, E.; Schapiro, I.; Melaccio, F.; Glusac, K. D.; Olivucci, M. A Conical Intersection Controls the Deactivation of the Bacterial Luciferase Fluorophore. *Angew. Chem. Int. Ed.* **2014**, *53*, 9870-9875.
(46) Brettel, K.; Byrdin, M. Reaction Mechanisms of DNA Photolyase. *Curr. Opin. Struct. Biol.* **2010**, *20*, 693-701.
(47) Yamamoto, J.; Plaza, P.; Brettel, K. Repair of (6-4) Lesions in DNA by (6-4) Photolyase: 20 Years of Quest for the Photoreaction Mechanism. *Photochem. Photobiol.* **2017**, *93*, 51-66.
(48) Porter, D. J. T.; Voet, J. G.; Bright, H. J. Direct Evidence for Carbanions and Covalent N5-Flavin-Carbanion Adducts as Catalytic Intermediates in the Oxidation of Nitroethane by d-Amino Acid Oxidase. *J. Biol. Chem.* **1973**, *248*, 4400-4416.
(49) Ghisla, S.; Massey, V.; Choong, Y. S. Covalent Adducts of Lactate Oxidase. Photochemical Formation and Structure Identification. *J. Biol. Chem.* **1979**, *254*, 662-669.
(50) Soltero-Higgin, M.; Carlson, E. E.; Gruber, T. D.; Kiessling, L. L. A Unique Catalytic Mechanism for UDP-Galactopyranose Mutase. *Nat. Struct. Mol. Biol.* **2004**, *11*, 539-543.
(51) Razeto, A.; Mattiroli, F.; Carpanelli, E.; Aliverti, A.; Pandini, V.; Coda, A.; Mattevi, A. The Crucial Step in Ether Phospholipid Biosynthesis: Structural Basis of a Noncanonical Reaction Associated with a Peroxisomal Disorder. *Structure* **2007**, *15*, 683-692.
(52) Payne, K. A. P.; White, M. D.; Fisher, K.; Khara, B.; Bailey, S. S.; Parker, D.; Rattray, N. J. W.; Trivedi, D. K.; Goodacre, R.; Beveridge, R. et al. New Cofactor Supports α,β-Unsaturated Acid Decarboxylation Via 1,3-Dipolar Cycloaddition. *Nature* **2015**, *522*, 497-501.
(53) White, M. D.; Payne, K. A. P.; Fisher, K.; Marshall, S. A.; Parker, D.; Rattray, N. J. W.; Trivedi, D. K.; Goodacre, R.; Rigby, S. E. J.; Scrutton, N. S. et al. UbiX Is a Flavin Prenyltransferase Required for Bacterial Ubiquinone Biosynthesis. *Nature* **2015**, *522*, 502-506.
(54) Hamdane, D.; Grosjean, H.; Fontecave, M. Flavin-Dependent Methylation of RNAs: Complex Chemistry for a Simple Modification. *J. Mol. Biol.* **2016**, *428*, 4867-4881.
(55) Mishanina, T. V.; Yu, L.; Karunaratne, K.; Mondal, D.; Corcoran, J. M.; Choi, M. A.; Kohen, A. An Unprecedented Mechanism of Nucleotide Methylation in Organisms Containing ThyX. *Science* **2016**, *351*, 507-510.

(56) Leys, D. Flavin Metamorphosis: Cofactor Transformation through Prenylation. *Curr. Opin. Chem. Biol.* **2018**, *47*, 117-125.
(57) Marshall, S. A.; Payne, K. A. P.; Fisher, K.; White, M. D.; Ní Cheallaigh, A.; Balaikaite, A.; Rigby, S. E. J.; Leys, D. The UbiX Flavin Prenyltransferase Reaction Mechanism Resembles Class I Terpene Cyclase Chemistry. *Nat. Commun.* **2019**, *10*, 2357.
(58) Beaupre, B. A.; Moran, G. R. N5 Is the New C4a: Biochemical Functionalization of Reduced Flavins at the N5 Position. *Frontiers in Molecular Biosciences* **2020**, *7*, 598912.
(59) Binda, C.; Valente, S.; Romanenghi, M.; Pilotto, S.; Cirilli, R.; Karytinos, A.; Ciossani, G.; Botrugno, O. A.; Forneris, F.; Tardugno, M. et al. Biochemical, Structural, and Biological Evaluation of Tranylcypromine Derivatives as Inhibitors of Histone Demethylases LSD1 and LSD2. *J. Am. Chem. Soc.* **2010**, *132*, 6827-6833.
(60) Bou-Nader, C.; Cornu, D.; Guerineau, V.; Fogeron, T.; Fontecave, M.; Hamdane, D. Enzyme Activation with a Synthetic Catalytic Co-Enzyme Intermediate: Nucleotide Methylation by Flavoenzymes. *Angew. Chem. Int. Ed.* **2017**, *56*, 12523-12527.
(61) Bou-Nader, C.; Stull, F. W.; Pecqueur, L.; Simon, P.; Guérineau, V.; Royant, A.; Fontecave, M.; Lombard, M.; Palfey, B. A.; Hamdane, D. An Enzymatic Activation of Formaldehyde for Nucleotide Methylation. *Nat. Commun.* **2021**, *12*, 4542.
(62) Lacombat, F.; Plaza, P.; Plamont, M. A.; Espagne, A. Photoinduced Chromophore Hydration in the Fluorescent Protein Dreiklang Is Triggered by Ultrafast Excited-State Proton Transfer Coupled to a Low-Frequency Vibration. *J. Phys. Chem. Lett.* **2017**, *8*, 1489-1495.
(63) van Stokkum, I. H. M.; Delmar, S. L.; van Grondelle, R. Global and Target Analysis of Time-Resolved Spectra. *Biochim. Biophys. Acta Bioenerg.* **2004**, *1657*, 82-104.
(64) *Gaussian 16, Revision C.01*. Frisch, M. J.; Trucks, G. W.; Schlegel, H. B.; Scuseria, G. E.; Robb, M. A.; Cheeseman, J. R.; Scalmani, G.; Barone, V.; Petersson, G. A.; Nakatsuji, H. et al.; Gaussian, Inc.: Wallingford CT, 2016.
(65) Yanai, T.; Tew, D. P.; Handy, N. C. A New Hybrid Exchange–Correlation Functional Using the Coulomb-Attenuating Method (CAM-B3LYP). *Chem. Phys. Lett.* **2004**, *393*, 51-57.
(66) Grimme, S.; Ehrlich, S.; Goerigk, L. Effect of the Damping Function in Dispersion Corrected Density Functional Theory. *J. Comput. Chem.* **2011**, *32*, 1456-1465.
(67) Dunning, T. H., Jr. Gaussian Basis Sets for Use in Correlated Molecular Calculations. I. The Atoms Boron through Neon and Hydrogen. *J. Chem. Phys.* **1989**, *90*, 1007-1023.
(68) Spicher, S.; Plett, C.; Pracht, P.; Hansen, A.; Grimme, S. Automated Molecular Cluster Growing for Explicit Solvation by Efficient Force Field and Tight Binding Methods. *J. Chem. Theory Comput.* **2022**, *18*, 3174-3189.
(69) Grimme, S. Exploration of Chemical Compound, Conformer, and Reaction Space with Meta-Dynamics Simulations Based on Tight-Binding Quantum Chemical Calculations. *J. Chem. Theory Comput.* **2019**, *15*, 2847-2862.
(70) Pracht, P.; Bohle, F.; Grimme, S. Automated Exploration of the Low-Energy Chemical Space with Fast Quantum Chemical Methods. *Phys. Chem. Chem. Phys.* **2020**, *22*, 7169-7192.
(71) Bannwarth, C.; Caldeweyher, E.; Ehlert, S.; Hansen, A.; Pracht, P.; Seibert, J.; Spicher, S.; Grimme, S. Extended Tight-Binding Quantum Chemistry Methods. *Wiley Interdiscip. Rev. Comput. Mol. Sci.* **2021**, *11*, e1493.
(72) *Gaussview, Version 5.0*. Dennington, R.; Keith, T. A.; Millam, J. M.; Semichem Inc.: Shawnee Mission KS, 2016.
(73) Kozlowski, D.; Pilmé, J. New Insights in Quantum Chemical Topology Studies Using Numerical Grid-Based Analyses. *J. Comput. Chem.* **2011**, *32*, 3207-3217.
(74) Chevreau, H.; Pilmé, J. Promising Insights in Parallel Grid-Based Algorithms for Quantum Chemical Topology. *J. Comput. Chem.* **2023**, *44*, 1505-1516.
(75) Glendening, E. D.; Landis, C. R.; Weinhold, F. NBO 6.0: Natural Bond Orbital Analysis Program. *J. Comput. Chem.* **2013**, *34*, 1429-1437.

(76) Kabir, M. P.; Orozco-Gonzalez, Y.; Gozem, S. Electronic Spectra of Flavin in Different Redox and Protonation States: A Computational Perspective on the Effect of the Electrostatic Environment. *Phys. Chem. Chem. Phys.* **2019**, *21*, 16526-16537.
(77) Hamdane, D.; Argentini, M.; Cornu, D.; Golinelli-Pimpaneau, B.; Fontecave, M. FAD/Folate-Dependent tRNA Methyltransferase: Flavin as a New Methyl-Transfer Agent. *J. Am. Chem. Soc.* **2012**, *134*, 19739-19745.
(78) Kar, R. K.; Borin, V. A.; Ding, Y.; Matysik, J.; Schapiro, I. Spectroscopic Properties of Lumiflavin: A Quantum Chemical Study. *Photochem. Photobiol.* **2019**, *95*, 662-674.
(79) Kar, R. K.; Miller, A.-F.; Mroginski, M.-A. Understanding Flavin Electronic Structure and Spectra. *WIREs Computational Molecular Science* **2022**, *12*, e1541.
(80) Martin, R. L. Natural Transition Orbitals. *J. Chem. Phys.* **2003**, *118*, 4775-4777.
(81) Greco, C.; Moro, G.; Bertini, L.; Biczysko, M.; Barone, V.; Cosentino, U. Computational Investigation on the Spectroscopic Properties of Thiophene Based Europium β-Diketonate Complexes. *J. Chem. Theory Comput.* **2014**, *10*, 767-777.
(82) Ghisla, S.; Hartmann, U.; Hemmerich, P.; Müller, F. Studien in Der Flavin-Reihe, XVIII. Die Reduktive Alkylierung Des Flavinkerns; Struktur Und Reaktivität Von Dihydroflavinen. *Justus Liebigs Annal. Chem.* **1973**, 1388-1415.
(83) Jarzeba, W.; Walker, G. C.; Johnson, A. E.; Kahlow, M. A.; Barbara, P. F. Femtosecond Microscopic Solvation Dynamics of Aqueous Solutions. *J. Phys. Chem.* **1988**, *92*, 7039-7041.
(84) Jimenez, R.; Fleming, G. R.; Kumar, P. V.; Maroncelli, M. Femtosecond Solvation Dynamics of Water. *Nature* **1994**, *369*, 471-473.
(85) Gilbert, A.; Baggott, J. E. *Essentials of Molecular Photochemistry*; Blackwell Science Ltd.: Oxford, 1991.

FIGURES

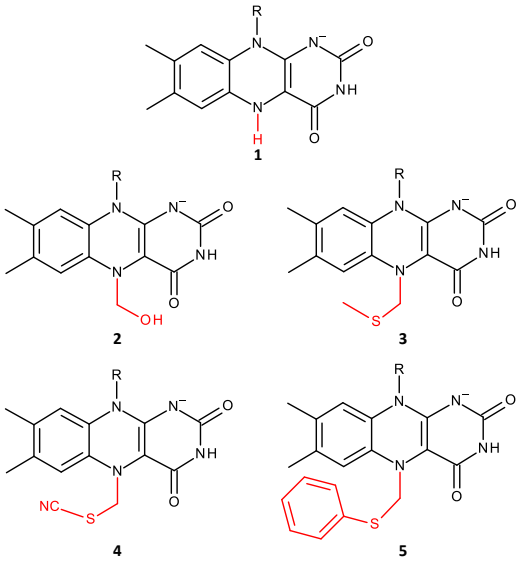

Fig. 1. Chemical structure of $FADH^-$ (**1**) and corresponding N_5-adducts (**2** to **5**). R stands for ribityl adenosine diphosphate. The lumiflavin analogs (R = CH_3) used for *ab initio* calculations are noted with primed numbers (**1'**, **2'**, **3'**).

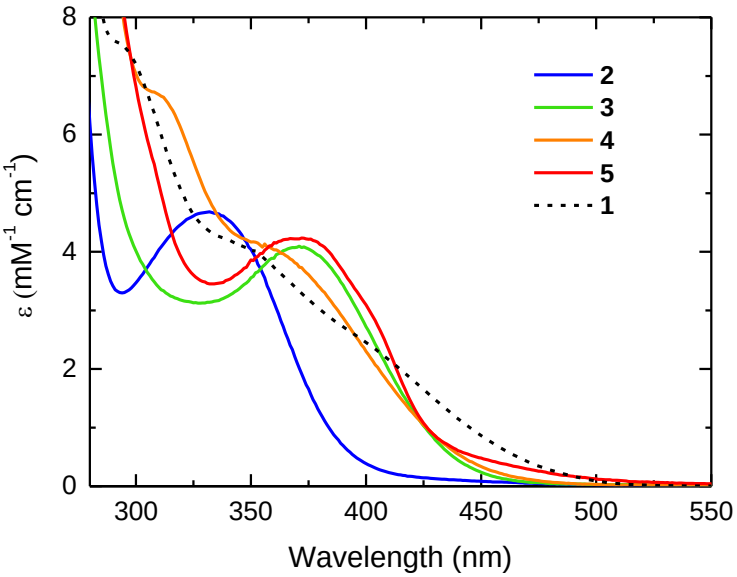

Fig. 2. Steady-state absorption spectra of the N_5-adducts (**2**, blue; **3**, green; **4**, orange; **5**, red) studied in this work, in aqueous solution (50/50 % vol. water-acetonitrile mixture for **5**) and $FADH^-$ (**1**, black in dotted line, (reproduced from Dozova *et al.*,[34] with permission from the PCCP Owner Societies).

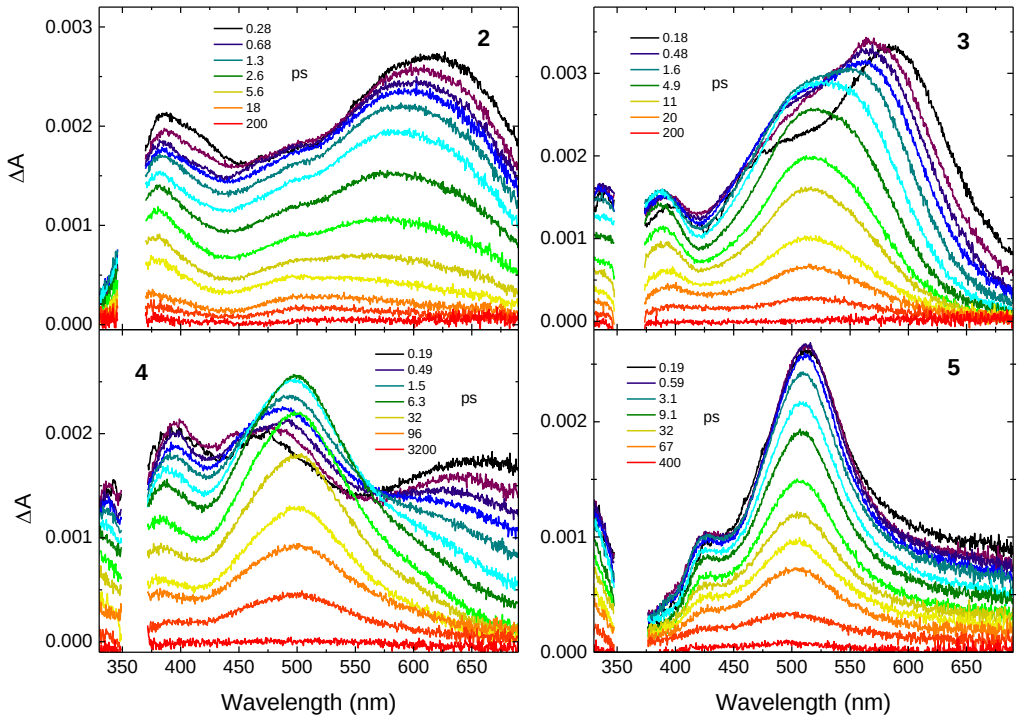

Fig. 3. Femtosecond transient absorption spectra of **2**, **3**, **4** and **5** (see notations in the Introduction) in solution at selected pump-probe delays, upon excitation at 360 nm.

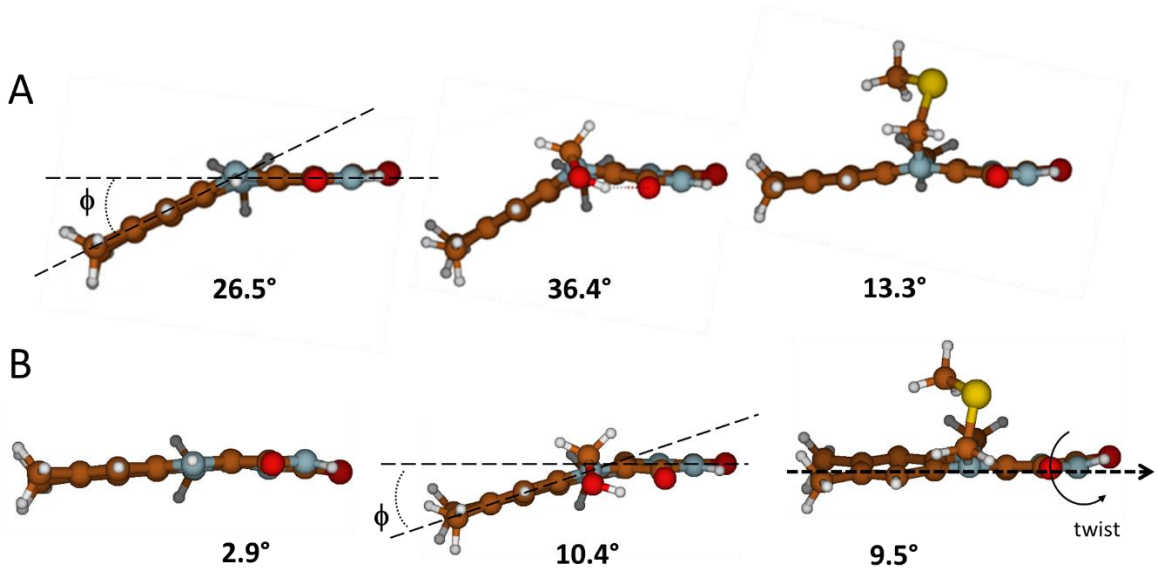

Fig. 4. Optimized structures of the lumiflavin derivatives **1'**, **2'** and **3'** and angle of dihedral bend ϕ calculated with explicit solvation (PBE1PBE/6-311++g(d,p)) in the ground state (A) and the first excited state ES_1 (B). An additional deformation of **3'** (a twist around the long axis of the molecule) is clearly visible in the excited state of **3'**.

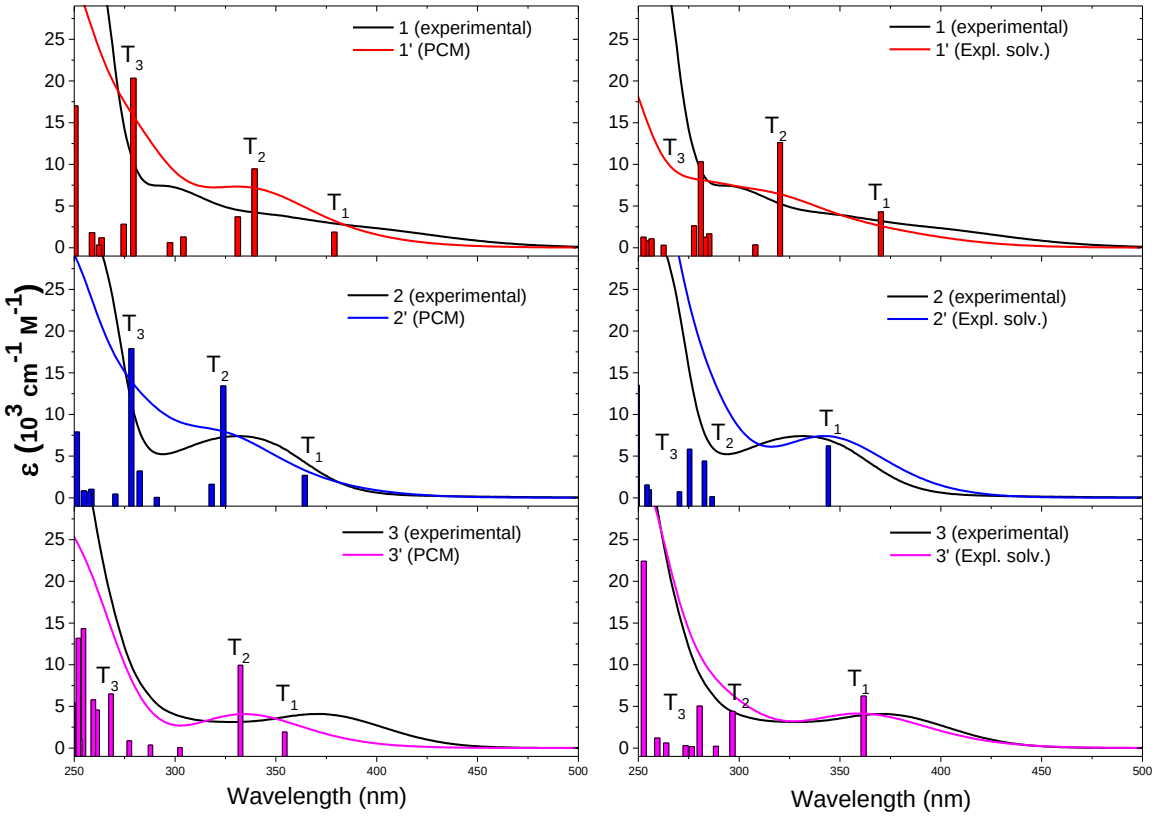

Fig. 5. Simulated UV-visible absorption spectra of lumiflavin derivatives **1'**, **2'** and **3'** by TDDFT PBE1PBE/6-311++g(d,p) calculations with implicit solvation (left) and explicit solvation (right). Corresponding experimental spectra are also reported. Intensities of simulated spectra have been normalized for comparison with experimental data. (The T_i symbol describes an allowed transition from the ground singlet state S_0 to an excited singlet state.)

Table 1. Time constants (τ_i in ps, with fit errors)of the global multiexponential analysis of the different systems under study. The last line recalls for reference the case of free $FADH^-$ (**1**) in aqueous solution, under the same experimental conditions (as published in Ref. [34]).

Molec.	τ_1 (ps)	τ_2 (ps)	τ_3 (ps)	τ_4 (ps)	plateau
2	0.37 ± 0.13	1.1 ± 0.3	2.2 ± 0.2	29 ± 2	no
3	0.61 ± 0.2	2.8 ± 0.3	10.1 ± 0.2	–	yes
4	1.5 ± 0.2	14 ± 3	50 ± 7	227 ± 38	no
5	0.31 ± 0.06	5.9 ± 0.8	35 ± 5	184 ± 25	no
1	0.27 ± 0.04	1.5 ± 0.1	8.4 ± 0.7	32 ± 1	yes

Table 2. Time constants (τ_i in ps) of the multiexponential analysis of the integral decay traces. The corresponding relative amplitudes (a_i) are indicated in parentheses. The bottom line refers to **1** as published in Ref. [34].

Molec.	τ_1 (a_1)	τ_2 (a_2)	τ_3 (a_3)	τ_4 (a_4)	plateau
2	3.6 (0.90)	77 (0.10)	–	–	–
3	11 (0.98)	271 (0.01)	–	–	(0.01)
4	0.28 (0.04)	18 (0.26)	57 (0.46)	227 (0.24)	–
5	5.1 (0.20)	34 (0.47)	185 (0.33)	–	–
1	2.0 (0.21)	10.9 (0.35)	35 (0.42)	–	(0.02)

Table 3. Average decay time ($\overline{\tau}$) and standard deviation of decay times (σ) calculated from the multiexponential fit of the integral decay traces. Ratios of $\overline{\tau}$ relative to **1** are provided in the last column.

Molec.	$\overline{\tau}$ (ps)	σ(ps)	$\overline{\tau}/\overline{\tau}_{ref}$
2	11	22	0.55
3	15	32	0.80
4	85	82	4.5
5	78	76	4.1
1 (ref.)	19	14	1

ASSOCIATED CONTENT

Supplementary information:

The following files are available free of charge.

- Transient absorption spectra of $FADH^{\cdot}$; Transient absorption spectra and integrated decay times of the N_5 adducts; Calculated geometries, dihedral angles and Cartesian coordinates; Calculated UV-visible spectra and transition wavelengths; Natural Transition Orbitals (NTO); Transition energy diagrams; Energies of the HOMO calculated with or without water molecules; Charge distribution; Adiabatic energies, oscillator strengths and transition electric dipole moments (PDF)

AUTHOR INFORMATION

Corresponding Authors

*Nadia Dozova: Email: nadia.dozova@sorbonne-universite.fr. Phone: +33 144322416.

*Djemel Hamdane: Email: djemel.hamdane@sorbonne-universite.fr. Phone: +33 44271254.

*Bruno Madebene: Email: bruno.madebene@sorbonne-universite.fr. Phone: +33 144273024.